PLEISTOCENE SHELF-MARGIN DELTA: INTRADELTAIC DEFORMATION AND SEDIMENT BYPASS, NORTHERN GULF OF MEXICO

A Thesis

Presented to

the Faculty of the Department of Earth and Atmospheric Sciences

University of Houston

In Partial Fulfillment

of the Requirements for the Degree

Master of Science

By

Grigoriy Perov

May 2009

PLEISTOCENE SHELF-MARGIN DELTA: INTRADELTAIC DEFORMATION AND SEDIMENT BYPASS, NORTHERN GULF OF MEXICO

_____

Grigoriy Perov

APPROVED:

_____

Dr. Janok P. Bhattacharya, Chairman

_____

Dr. Christopher Liner

_____

Mr. John Sharp

_____

Dr. Kurt Marfurt

_____

Dean, College of Natural Sciences and Mathematics

ACKNOWLEDGEMENTS

PLEISTOCENE SHELF-MARGIN DELTA: INTRADELTAIC DEFORMATION AND SEDIMENT BYPASS, NORTHERN GULF OF MEXICO

An Abstract of a Thesis

Presented to

the Faculty of the Department of Earth and Atmospheric Sciences

University of Houston

In Partial Fulfillment

of the Requirements for the Degree

Master of Science

By

Grigoriy Perov

May 2009

ABSTRACT

3D seismic data allow evaluation of soft-sediment deformation features in a Pleistocene shelf-margin delta within a salt dome mini-basin, offshore Louisiana. The delta consists of a series of offlapping sandy clinoforms, interpreted as being associated with a prolonged forced regression and ensuing lowstand of sea level, associated with Oxygen isotope stage 6, which lasted for about 20Ky. The lowstand delta is onlapped by a transgressive mud wedge, and is underlain and capped by regionally persistent highstand mudstones. The central part of the delta shows severe disruption, suggestive of soft-sediment deformation. Two types of deformation are observed. Syn-sedimentary intra-deltaic deformation is indicated by a series of slumps and growth faults. The central part of the delta also shows post-depositional extradeltaic deformation caused by a shallow-water mass transport complex (MTC) that remobilizes the deltaic deposits. The MTC shows well defined pressure ridges and forms two lobate complexes that show clear truncation of the older clinoform delta deposits. Mapping of the MTCs shows that sediment transport was almost perpendicular to the direction of the regional delta progradation that it replaces. The shallow mass transport complex is interpreted to have formed in water depths of around 100 m and was likely induced by the uplift of the adjacent western salt dome. Tributive channels downdip of the delta front are interpreted as submarine slope channels, some of which are connected with distributary channels, probably forming near the end of the prolonged lowstand. These channels have a high potential for transporting coarse-grained sediment down the slope and onto the basin floor.

We hypothesize that the high degree of syn- and post-depositional deformation, as well as the well developed shelf-edge channel network, are related to the prolonged nature of the lowstand. In contrast, shelf-edge deltas formed during shorter-term eustatic drops seem to lack the deformation features.

CONTENTS

INTRODUCTION

Deltas are the key element in the building of constructional shelves and shelf margins. The geomorphic and internal characteristics of deltas are important for predicting of sand partitioning across the shelf and onto slope and basinal settings. Shelf-margin deltas are an important yet understudied type of depositional environment. Recent studies of shelf-margin deltas in the Gulf of Mexico, (Anderson et al., 2004; Wellner et al., 2004; Roberts et al., 2004; Abdulah et al., 2004) focused on 2D seismic datasets and lacked 3D seismic representation of lithology distribution, deformation features, and therefore reservoir quality.

Traditional literature (Bhattacharya and Walker, 1992; Coleman and Wright, 1975; Galloway, 1975) suggests that external morphology is highly indicative of the depositional processes and internal facies architecture of deltas. Many recent studies suggest that the overall smooth, lobate shape of shelf-edge deltas, as typically mapped in seismic data, indicates a wave-dominated character (Porebski and Steel, 2002, 2006; Abdulah et al., 2004). These predictions are largely based on the gross mapping of the overall delta complexes with very little data about the internal geomorphology or facies. However more recent work, (Rodriguez et al., 2000; Fielding et al., 2005; Bhattacharya, 2006; Gani and Bhattacharya, 2007), shows smooth-fronted lobate deltas that nevertheless, have more river- or tide-influenced internal facies. The Lagniappe delta, despite a locally lobate geometry and smooth front, internally shows a plethora of small-scale mouth bars, bar assemblages, and many terminal distributary channels, suggesting river-dominance, (Roberts et al., 2004). External morphology may not necessarily be a

good predictor of internal facies architecture. 3D seismic data allows the elucidation of the internal architecture of delta lobes.

The focus of this project is to examine the geomorphology and internal facies architecture of a shelf-margin delta in a salt dome minibasin, within the Gulf of Mexico using 3D seismic data. Syn- and post-depositional deformation is documented to provide an example of the reservoir complexity within a shelf margin system. The 3D data also allows an evaluation of the potential processes and pathways for sediment bypass from delta front to slope and deep water depositional environments.

GEOLOGICAL SETTING

The study area (Fig. 1) is in the Northern Gulf of Mexico, 100 km south of Louisiana, and covers the shelf margin and upper slope. Water depths are between 80 and 120 meters. The shelf is around 80 km wide at this location.

The Gulf basin originated during Jurassic by rifting accompanied by salt deposition (Salvador, 1987; Diegel et al., 1995). The Texas-Louisiana continental shelf and slope environments are dominated by salt tectonics. Accommodation in the northern Gulf of Mexico is controlled by eustatic sea-level fluctuations, geothermal subsidence, local subsidence caused by salt withdrawal, large scale growth faulting, and sedimentary compaction (Winker and Edwards, 1983). Eustatic sea-level curves are well established for Pleistocene and Holocene times, Fig. 2 (Imbrie, 1979). Subsidence rates on the shelf increase almost linearly in the basinward direction, ranging from 0.1 mm/year on the inner shelf to 4 mm/year on the outer shelf (Anderson et al., 2004). Thick salt deposits were remobilized by massive sediment loads transported by river-delta systems from the peripheral drainage areas during the Cenozoic. Upwelling salt massifs create additional accommodation in the form of minibasins, which trap sediments from the advancing deltas (Alexander and Flemings, 1995). During the Pleistocene, the Paleo-Mississippi river system supplied sediments to the northern Gulf of Mexico (Galloway et al., 2000).
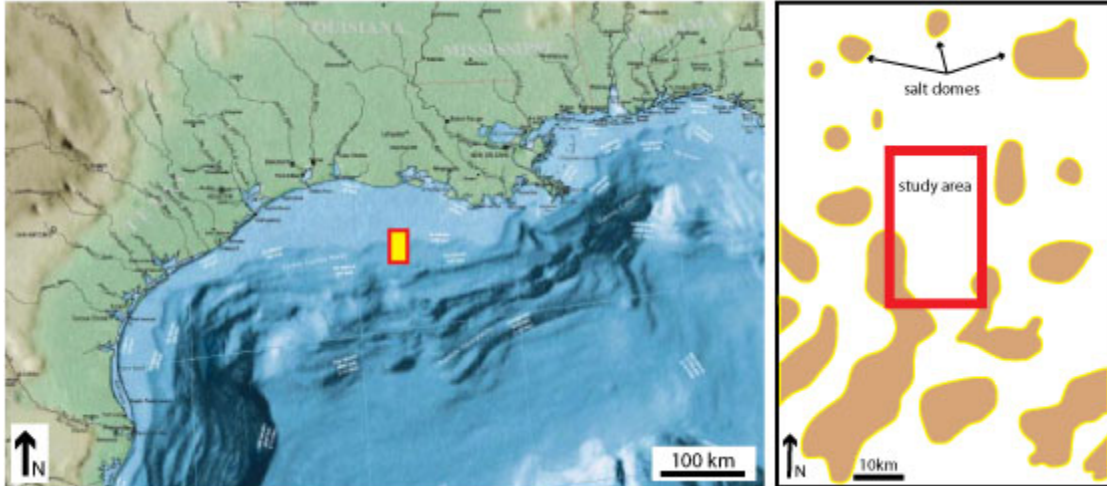
Figure 1. Left: Regional bathymetry map of the Gulf of Mexico. The location of the seismic survey is shown with yellow rectangle, source: http://www.portpublishing.com/Computer%20Based/GULFO%20retail%20order.html.

Right: A map of salt domes (brown) in the vicinity of the seismic survey (red rectangle), redrawn from Berryhill et al., 1986.
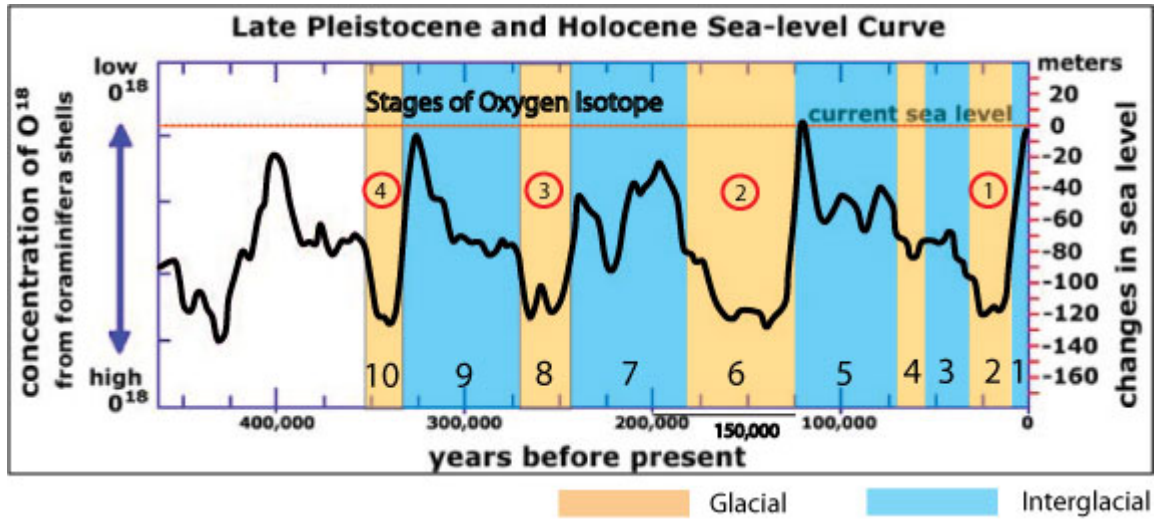
Figure 2. Eustatic sea-level curve for Late Pleistocene and Holocene. Also shown are Oxygen isotope stages 1 to 10, and suggested timing of the deposition of deltaic complexes 1 through 4 from the Figure 4.

DATA AND METHODS

The 3D seismic data used for this study are part of a prestack migrated seismic survey 8000 km^2 in area, acquired by Petroleum Geo-Sciences (PGS) and donated to the University of Houston. We are using 473 km^2 covering the southeastern corner of the south addition of Vermilion block, and the northern part of the Garden Banks block. The survey is enclosed between latitudes 27° 50' N – 28° 10' N and longitudes 92° 11' W – 92° 23' W. The in-line and cross-line lengths are 24,750 m and 19,125 m respectively. Horizontal resolution is defined by the distance between in-lines (25 m) and cross-lines (37.5 m). The 3D volume used in this research is limited to one-second, two-way travel time. Seismic velocities of 1550 m/s were used to convert two-way travel times into depth units (Wellner et al., 2004), and in calculations of the thicknesses of geologic elements. Vertical resolution of about 12 m is calculated using the dominant frequency of 35 Hz, (Chris Liner, University of Houston, personal communication, 2008), and the average velocity in the interval of interest. The 3D seismic survey used in this research overlaps the southeastern corner of the seismic data used by Wellner et al., 2004, allowing their chronostratigraphic observations to be tied to our dataset. Well log and core data are unavailable for the interval of interest. Petrel software was used for seismic interpretation. Reflection amplitude, as well as several other seismic attributes, such as coherence, variance, dip magnitude, and dip azimuth, were used for the interpretation of horizontal displays of seismic data, whereas vertical displays are exclusively interpreted on reflection amplitude.

We used the standard approach to the stratigraphic interpretation of the seismic data which includes the following steps:

- Data reconnaissance through successive vertical and horizontal slicing and movies, including diagonal and polyline intersections;

- Picking faults using coherence timeslices and interpreting surfaces and sequence boundaries, based on lapout relationships of seismic reflections;

- Interpolating horizons and creating contour and isochron maps;

- Extracting reflection amplitude and other attributes along or in the window attached to the interpolated horizons, parallel slicing, and/or time slicing of the flattened seismic volume along the interpreted horizons, thus removing the effect of structural deformation in order to investigate the seismic geomorphology of the various stratigraphic units;

- Defining seismic facies and mapping the extent and time thickness of the units to document facies and lithologic variability.

Our seismic stratigraphic, seismic facies, and chronostratigraphic analyses are based on the approach of Vail and Mitchum (1977) and Posamentier and Allen, (1999). The key to seismic data analysis in this study is recognition of geological features both in plan and section view. Observation of the geomorphic features on horizontal displays allows depiction of buried landforms, thereby greatly facilitating the 3D interpretation. Recent publications, e.g. Davies et al., 2007; Wood, 2007 describe the geomorphological approach to the interpretation of seismic data that this research is based on.

One of the useful insights from the seismic interpretation procedure is that vertical exaggeration works very well to identify lapout patterns and clinoform characteristics, but tends to obscure deformation features. Channels were mapped from amplitude and

variance horizon slices. Channel paths are better recognized on amplitude slices, whereas lateral extents of the channels are more precisely seen on variance slices.

TECTONICS AND STRATIGRAPHY OF THE MINIBASINS

The minibasin of interest is bound by two curvilinear salt massifs to the west and to the east, and covers an area of 600 km^2 (Fig. 3). The uplift of the western salt dome is contemporaneous with the upper minibasin fill and occurred earlier than the eastern salt dome rise, as interpreted from the thickness changes of the sediment successions against the flanks of the salt domes and location of the minibasin axis (Berryhill, 1986). Faulting to the north and to the south is related to salt dome formation. The upper kilometer of the minibasin stratigraphic fill is mostly represented by cyclic deltaic complexes of Pleistocene to Holocene age, deposited during the last 500,000 years (Fig. 2, and 4). Figure 4 shows four deltaic complexes on the north-south oriented cross-section (see Fig. 3 for location). Clinoforms are present in all four deltaic complexes, but vary in height, length, continuity, and dip angles (Fig. 3). Complexes 1 and 3 are undeformed, whereas Complexes 2 and 4 exhibit various degrees of internal deformation, indicated by chaotic seismic reflections. Deformation exists on different scales and is hypothesized to be caused by both deltaic and non-deltaic processes. This research is focused on unraveling the seismic stratigraphy and internal architecture and deformation of Complex 2. Correlations with 2D seismic data of Berryhill (1986) and Wellner et al. (2004) show that the deltaic complex was formed during the Oxygen isotope stage 6 lowstand of eustatic sea level, between 180 and 125 ky BP (Fig. 2).
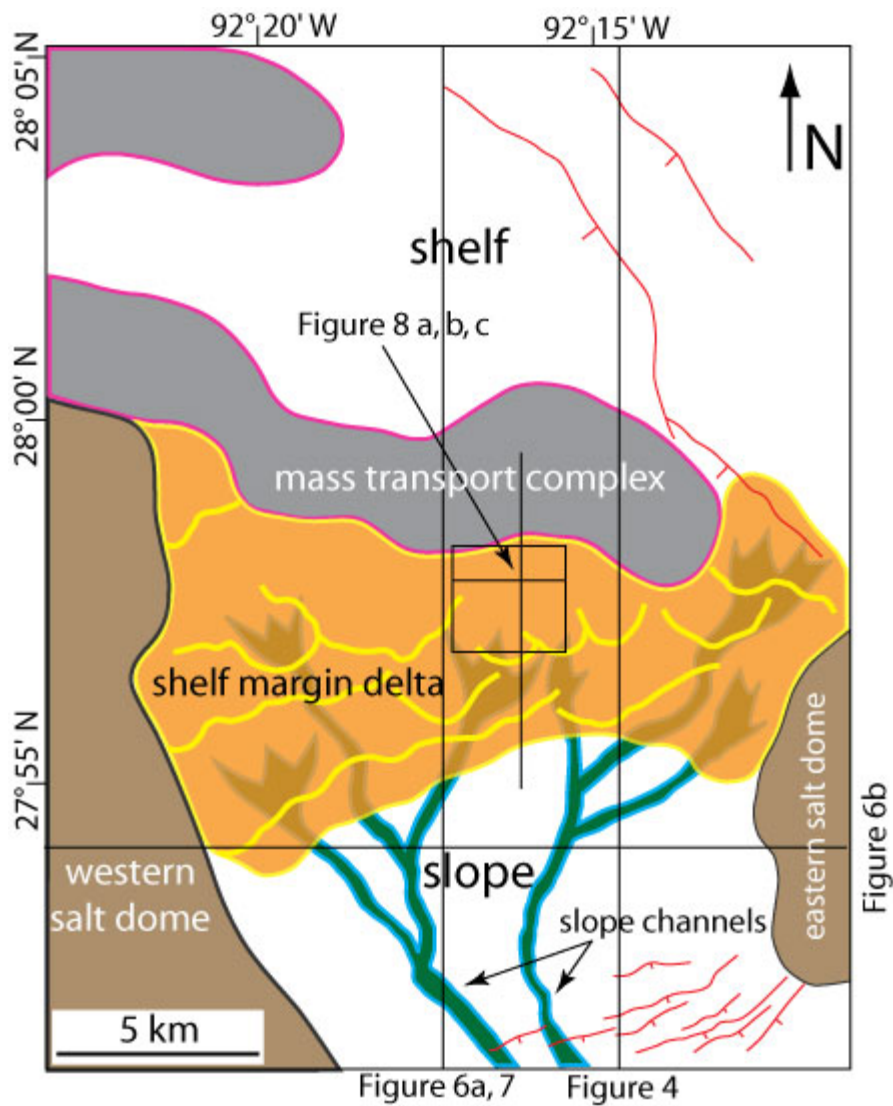
Figure 3. Schematic paleogeologic map of the study area. Main depositional elements include shelf-margin delta, mass transport complex and slope channels. Note the locations of seismic crosssections shown with grey lines.
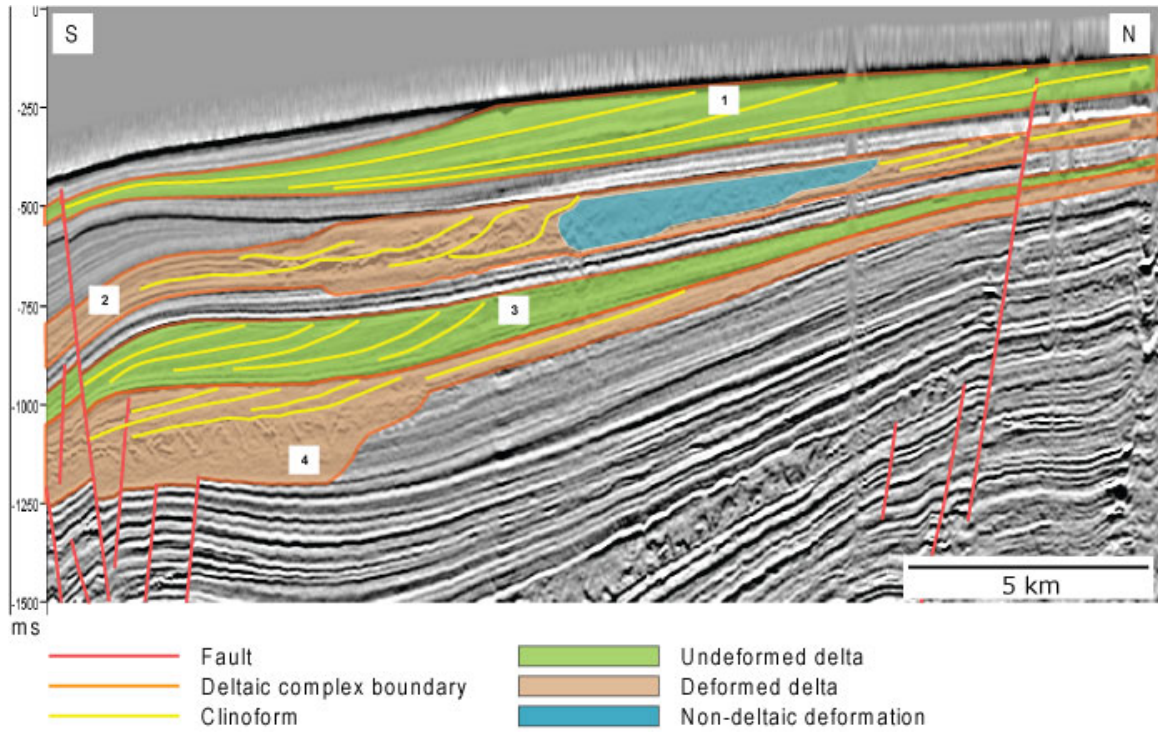
Figure 4. North-south oriented seismic amplitude crosssection showing four deltaic complexes comprising the upper second of the minibasin fill. Deltaic complexes show a cyclic character of deformation: Complex 1 and 3 are undeformed, whereas 2 and 4 are deformed. This study focuses on Complex 2.

SEISMIC FACIES, DEPOSITIONAL ENVIRONMENTS, AND LITHOLOGY DISTRIBUTION

Six seismic facies (Fig. 5) were defined on the basis of external geometry, reflection terminations at the depositional boundaries, amplitude, continuity, and internal geometry of reflections, (Mitchum et al., 1977). Depositional environments, processes, and resulting depositional elements are interpreted by comparing cross-sectional geometry and plan view geomorphological patterns with analog facies models for both modern and ancient depositional environments. Lithology distribution and connectivity are interpreted for each facies based primarily on reflection character and amplitude.
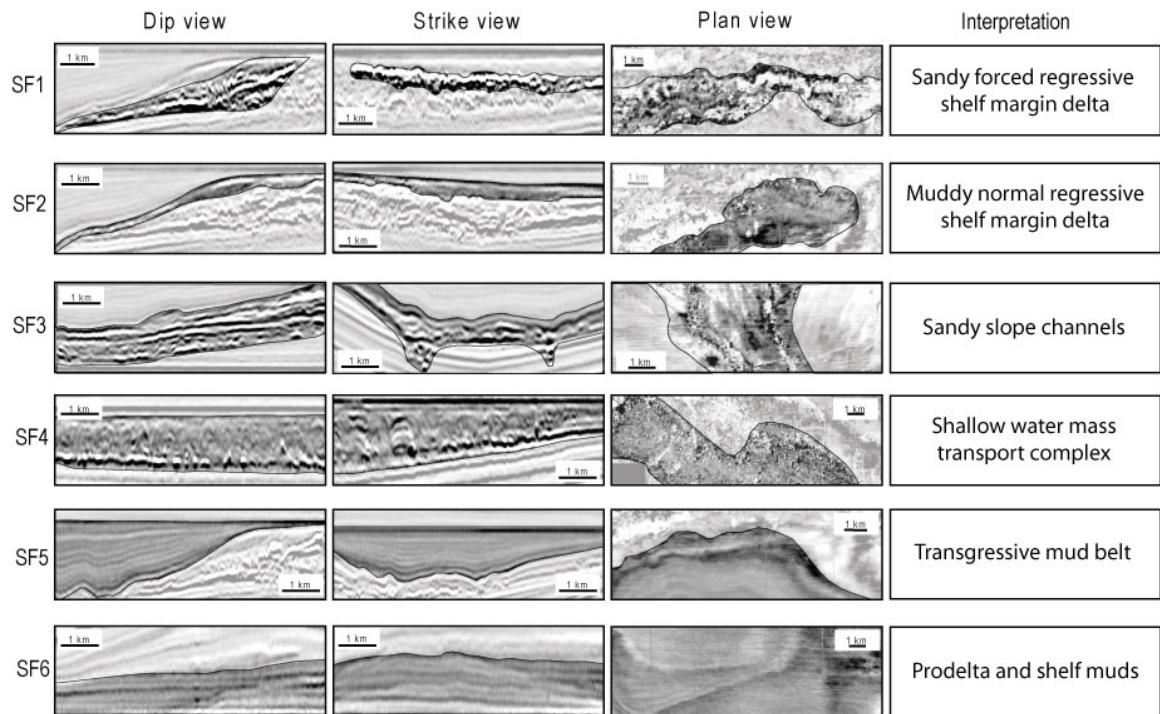
Figure 5. Six seismic facies (SF1-SF6) recognized in this study shown in dip, strike and plan view. Brief interpretation of the seismic facies is provided on the figure. See text for details.

Seismic Facies 1 (SF 1): Sandy forced regressive shelf-margin delta

Seismic facies 1 (Fig. 5) comprises high amplitude, prograding lenses of offlapping to downstepping, medium continuity, and oblique tangential clinoforms in dip view. Clinoforms dip at angles of up to 3.2 degrees, are up to 100m high and around 7km long. In strike view SF1 is represented by high amplitude, concordant, continuous, and parallel to subparallel reflections whereas, in plan view it shows high amplitude, convex basinward lobate features.

Multiple lobes in plan view and prograding clinoforms in dip view are comparable in size and geometry with the features of the Lagniappe delta described in Roberts et al. (2004) and Sydow and Roberts (1994). The lobate geometry suggests that internally the deltas consist of a series of mouth bars and bar assemblages; high amplitudes in this area are indicative of sand. Therefore, we interpret SF1 as a sandy shelf-margin deltaic system. The downstepping nature of the clinoforms indicates a negative shoreline trajectory (Helland-Hansen and Gjelberg, 1994; Posamentier and Allen, 1999; Bhattacharya, 2006), suggesting a forced regressive depositional environment. Clinoforms show medium continuity due to the deformation, as discussed below.

Seismic Facies 2 (SF 2): Muddy normal regressive shelf margin delta

Seismic Facies 2 (Fig. 5) shows medium to low amplitude prograding lenses of offlapping to aggradational, high continuity, sigmoid tangential clinoforms in dip view. Clinoforms dip at angles of up to 2.5 degrees and are up to 120 m high and about 7 km long. In strike view SF2 comprises medium to low amplitude, concordant, parallel

seismic reflections with irregular base and flat top. The plan view is characterized by low amplitude, convex basinward lobate features.

The lower amplitudes are indicative of a muddier lithology. Clinoform height, shape, and the aggrading nature suggest a shelf-margin position for the prograding delta with a positive shoreline trajectory (Bhattacharya, 2006; Posamentier and Allen, 1999; Helland-Hansen and Gjelberg, 1994). Lobate features in plan view suggest a river-dominated delta (Bhattacharya, 2006; Roberts et al., 2004 and Wellner et al., 2004). We thus interpret SF2 as a muddy shelf-margin delta deposited in a normal regressive environment.

Seismic Facies 3 (SF 3): Sandy slope channels

In strike view Seismic facies 3 (Fig. 5) is defined by high amplitude, V-shaped erosional features. Reflections inside the fill are of medium to low continuity, exhibit a wavy contorted to chaotic pattern with isolated multiple extremely high amplitude reflection couplets primarily at the base. The height of the fill varies from 30 to 80 m. Elevation of the top surface can be observed locally creating a bulge over the fill. In dip view SF3 shows high amplitude inclined reflections. Reflections are parallel and continuous. The plan view SF3 is characterized by high amplitude, straight to meandering channel-like features, exhibiting a convergent and tributive pattern. Channels can reach tens of kilometers in length.

The amplitudes of SF3 are the highest compared to all other seismic facies, indicative of the highest sand content encased within a shale matrix. The shape and depositional contacts at the base suggest incision. High amplitudes at the base of the fill suggest

isolated sand bodies enclosed and overlain by shale. We thus interpret SF3 as slope channels (e.g., Fig. 2) incised at the front of the prograding delta. Similar features have been described in seismic data by Posamentier and Kolla (2003) and Beaubouef and Friedmann (2000), and in outcrop data by Plink-Bjorklund and Steel (2005).

The high depth of incision suggests slope channel valleys, and multiple couplet reflections comprise a multistory fill. The bulge over the valley fill is caused by differential compaction and supports the idea of a coarser grained, sand-prone deposit.

Seismic Facies 4 (SF 4): Shallow water mass transport complex

Seismic facies 4 (Fig. 5) is identified by low amplitude sediment fill with erosional truncation at the base. Concordant reflections at the top are represented by discontinuous, contorted to chaotic medium amplitude seismic reflections, and rotated stratified blocks. In strike view SF4 displays erosional contacts both at the base and at the lateral margins of the sediment fill, overlain by concordant reflections. Internal characteristics are similar to the ones described in the dip view. SF4 in plan view (Fig. 5) shows low amplitude, curvilinear geomorphic features characterized by convex amplitude patterns in the direction of flow.

The low amplitude character suggests that the fill is dominantly composed of mud, with coarser grained rotated blocks. Contorted and chaotic seismic facies suggest deformation of sediments, consistent amplitude patterns in plan view show the direction of movement and indicate the type of deformation.

We interpret SF4 as a shallow water mass transport complex (MTC) composed of deformed mud, that supports sandy blocks, and was formed due to the local uplift of the

adjacent salt dome. Posamentier and Kolla (2003) and Moscardelli et al. (2006) described mass transport complexes in deeper water settings. This MTC exhibits similar seismic characteristics, except they are smaller in size and lack erosional grooves at the base. Prather et al. (1998) described shallow mass transport complexes analogous to the ones studied in this research.

Seismic Facies 5 (SF 5): Transgressive marine mud belt

Seismic facies 5 (Fig. 5) forms a low amplitude onlapping wedge of reflections with a concordant top, exhibiting high continuity and parallel to converging internal geometry. Thin, medium to high amplitude layers are observed at the lower depositional boundary. In strike view SF5 is characterized by an irregular base and concordant top, and shows continuous, low amplitude, parallel to subparallel internal reflections. In plan view SF5 shows a low amplitude, laterally extensive geomorphic feature paralleling the paleoshoreline.

Low amplitudes indicate muddy lithology. Onlap on the lower depositional boundary suggests the transgressive nature of the deposits. The high amplitude layer at the base is interpreted to represent a reworked transgressive coarse grained lag. Posamentier and Allen (1999), Wellner et al. (2004), and Abdulah et al. (2004) interpreted analogous seismic facies as marine muds. We interpret SF5 as a transgressive marine mud belt onlapping SF2 and SF1.

Seismic Facies 6 (SF 6): Highstand deltaic and shelf deposits

Seismic facies 6 (Fig. 5) comprises medium to low amplitude wedges of prograding and aggrading clinoforms in dip view. They dip at low angles (less than 1°), show tangential downlap at the base, and are toplapping to truncated at the top. The length of the clinoforms reaches 20 km, whereas the height is on the order of 30 m, significantly lower than SF1 and SF2 (Fig. 5). Reflections are continuous and subparallel. In strike view SF6 is characterized by low amplitude, concordant, parallel and continuous reflections. In plan view, the geomorphology displays large, convex basinward bulges .

The low amplitudes and lateral persistence indicate marine shale-prone deposits. The height, length, and shape of these clinoforms suggest that they form the distal muddy prodelta toes of the shelf-margin deltas deposited updip in shallower water. The lack of steep clinoforms suggests a largely aggradational component. The lobate geometry in plan view, suggests a point-sourced deltaic origin of these muddy facies, suggesting lobate prodelta mud belts. Shifting lobes indicate switching depocenters for marine mud in the prodelta setting. Similar seismic facies were interpreted as highstand deltas in Roberts et al. (2004), Wellner et al. (2004), and Anderson et al. (2004). We interpret SF6 to represent inner to midshelf prodelta consisting primarily of mud and very fine sand.

KEY SEQUENCE STRATIGRAPHIC SURFACES

Four key stratigraphic surfaces were identified on the basis of lapout and truncational relationships. They include a sequence boundary (SB), intra-lowstand sequence surface (ILSB), transgressive surface of erosion (TSE), and maximum flooding surface (MFS) (Fig.6a and Fig.6b).

Sequence boundary (SB1)

On the outer shelf and shelf margin, the lower sequence boundary (SB1) (Fig. 6a, 6b) is expressed by a discontinuous, irregular, primarily high amplitude seismic reflection, overlying truncated older highstand prodelta deposits (SF6) and underlying downlapping lowstand clinoforms of SF1 and SF2 (Fig. 5). On the upper slope, SB1 (Fig. 6a, 6b) is characterized by a deep incision surface underlying slope channels (SF3), and by a conformable reflection in the interfluve areas. SB1 (Fig. 6a) is an erosional surface separating the previous highstand systems tract 1 (HST1), represented by marine prodelta muds (SF6), from the overlying lowstand systems tract (LST), represented by forced (SF1) to normal (SF2) regressive deltas and slope channels (SF3), (Fig. 6a, 6b).

Intra-lowstand sequence boundary (ILSB)

The intra-lowstand sequence boundary (ILSB) is present at the basinward end of the cross-section (Fig.6a and 6b). It is characterized by a medium amplitude, irregular reflection separating sandy (SF1) and muddy (SF2) deltaic deposits. In a basinward direction, the ILSB (Fig. 6a, 6b) coincides with SB1 in the incised parts of the upper slope, and with the transgressive surface of erosion (TSE) along the interfluve areas (Fig.

18

6a, 6b). In the landward direction, the ILSB merges with the maximum flooding surface (MFS2, Fig.6a).

The amplitude pattern and nature of the clinoforms above and below the ILSB suggest an increase of the aggradation and a decrease in sand content across the surface. The ILSB is interpreted to separate the early from late lowstand systems tracts, and marks the end of relative sea-level fall.

Transgressive surface of erosion (TSE)

The transgressive surface of erosion is a high to medium amplitude continuous reflection, which grades into the maximum flooding surface in a landward direction (Fig. 6a, 6b). Lowstand deltaic deposits of SF1 and SF2 (Fig. 6) are either truncated or toplap underneath the TSE in the outer shelf and shelf-margin position. In the upper slope region, the TSE overlies slope channels of SF3 and merges with the ILFS in the interfluve areas (Fig.6a). Transgressive marine muds of SF5 onlap the TSE until it merges with the MFS updip.

The TSE indicates the onset of transgression. Erosion was likely due to wave reworking during the eustatic sea-level rise. The TSE is interpreted to separate the late lowstand systems tract (LLST), consisting of deltas (SF1, SF2) and slope channels (SF3), from the transgressive systems tract (TST), represented by marine muds (SF5).

Maximum flooding surface (MFS2)

The maximum flooding surface 2 (Fig, 6a and 6b) forms a smooth, continuous, high amplitude reflection that lies directly below prodelta muds of SF6. The low amplitude character of SF6 is indicative of muddy distal marine facies and the lateral

19

persistence of this low angle downlapping facies suggests that they belong to the highstand systems tract 2 (HST2, Fig. 6a). The MFS2 lies above the onlapping transgressive mud belt (SF5) in a basinward direction, and merges with the ILSB and TSE in a landward direction, where they overlie the lowstand deltas (SF1, SF2) and associated mass transport complex (SF4), (Fig. 6a, 6b).

The MFS2 is interpreted to be formed at the time of maximum transgression of the shoreline, and is characterized by hemipelagic to pelagic sedimentation creating an acoustic impedance contrast with the underlying coarser grained lowstand delta deposits. This is responsible for the high amplitude continuous nature of the reflection associated with this surface.
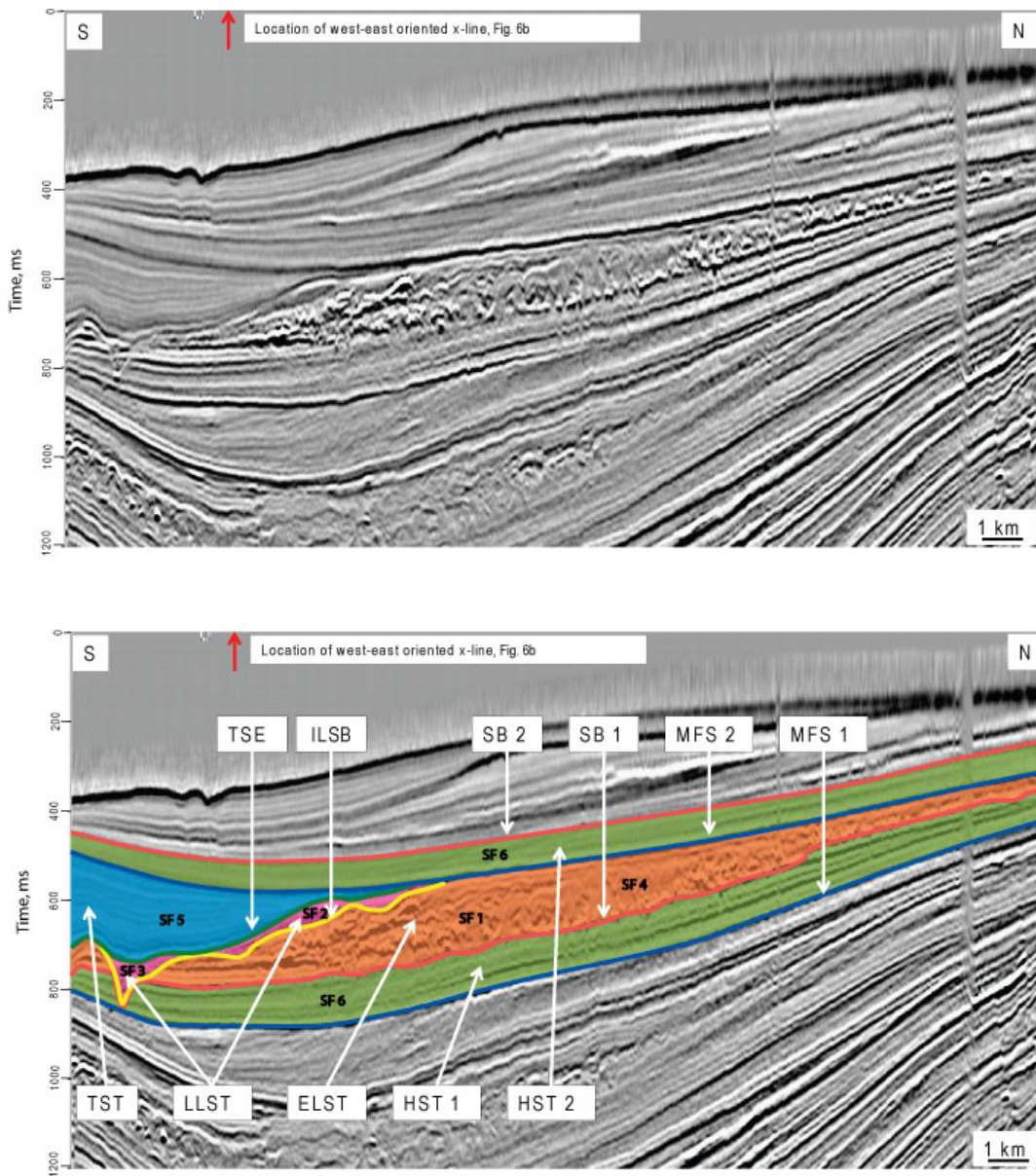
Figure 6 A. Uninterpreted and interpreted north-south oriented seismic amplitude cross section, see Figure 2 for location. Seismic facies, key stratigraphic surfaces, and systems tracts are labeled on the figure. MFS-maximum flooding surface, MFS-maximum flooding surface , SB-sequence boundary, TSE-transgressive surface of erosion, ILSB-Intra-lowstand sequence boundary, HST-Highstand systems tract, ELST-Early lowstand systems tract, LLST-Late lowstand systems tract, TST-Transgressive systems tract, SF1-6: Seismic facies 1-6.

21
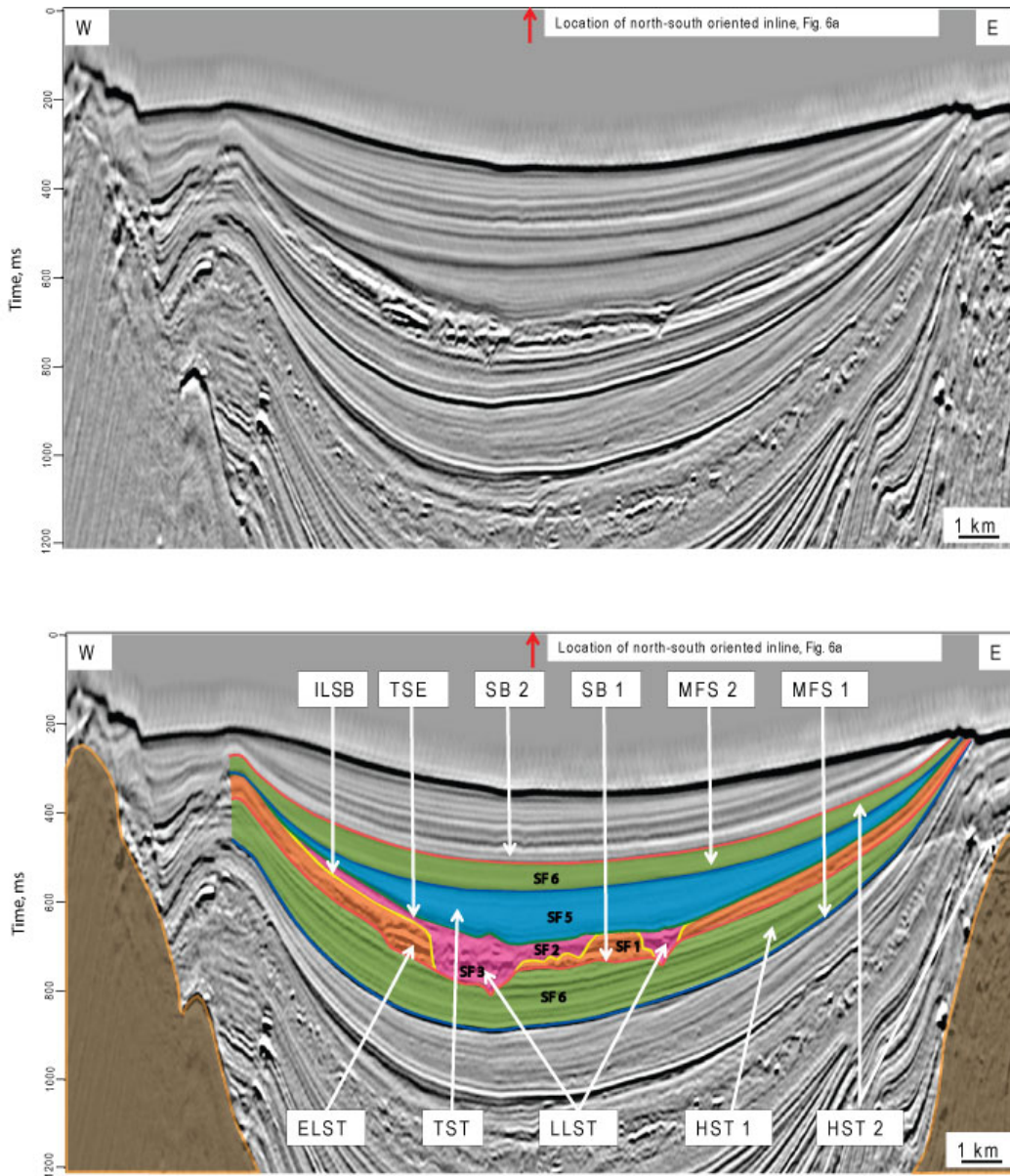
Figure 6 B. Uninterpreted and interpreted west-east oriented seismic amplitude cross section, see figure 2 for location. MFS-maximum flooding surface, MFS-maximum flooding surface , SB-sequence boundary, TSE-transgressive surface of erosion, ILSB-Intra-lowstand sequence boundary, HST-Highstand systems tract, ELST-Early lowstand systems tract, LLST-Late lowstand systems tract, TST-Transgressive systems tract, SF1-6: Seismic facies 1-6.

CHRONOSTRATIGRAPHY

Based on seismic facies and identification of key surfaces, the units under study can be divided into highstand, lowstand, and transgressive systems tracts. These are in turn tied to the eustatic sea-level curve (Fig. 7), which allows the construction of the chronostratigraphic chart of the north-south oriented cross section from the study area (Fig. 2 for location).
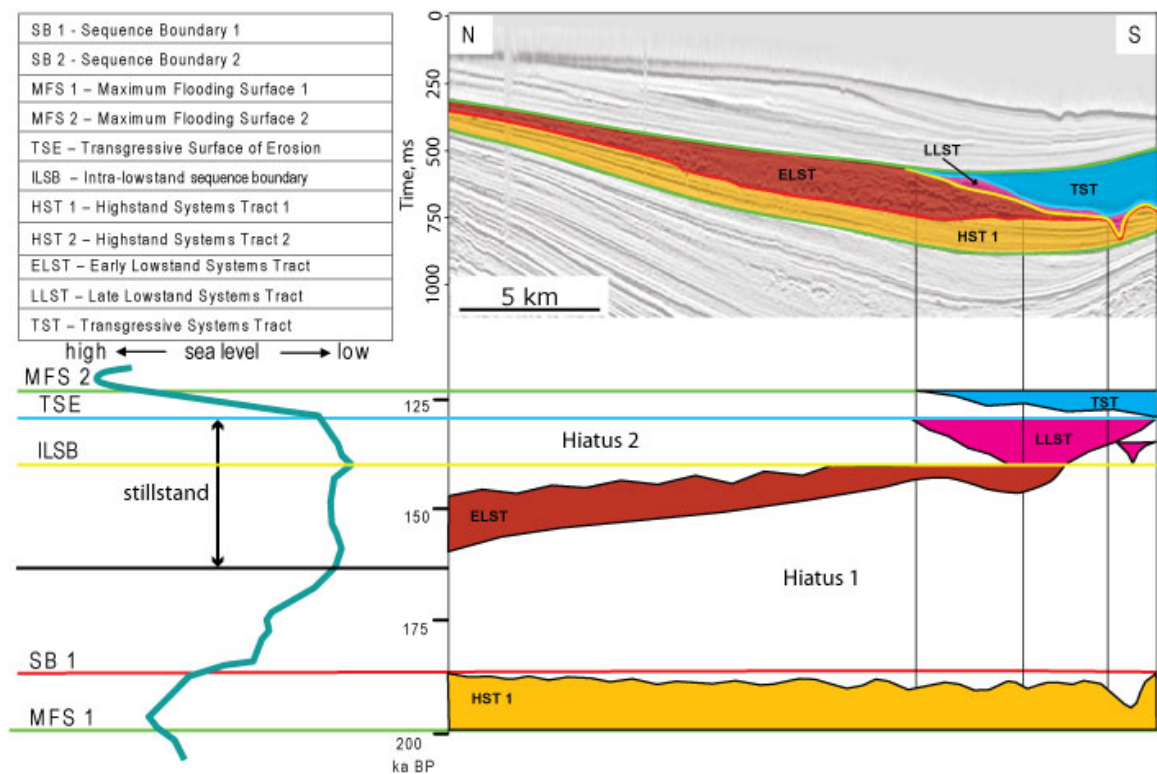
Figure 7. Schematic chronostratigraphic chart of delta complex 2 from Figure 4. Systems tracts are labeled and colored. The chart, also called a Wheeler's diagram was constructed to tie the timing of deposition of the complex 2 from Figure 4 to the eustatic sea-level curve from Figure 2.

200 to 185 ka BP, highstand systems tract (HST)

The highstand systems tract 1 (HST1) was formed during the period of increasing accommodation, when the rate of sediment supply was high enough to maintain the normal regression of the shoreline. It is underlain by the maximum flooding surface 1 (MFS 1) and overlain by the erosional sequence boundary 1 (SB1). The erosional vacuity increases basinward due to stronger erosion by delta-front channels, and a longer period of non-deposition prior to the formation of the lowstand delta. The HST is represented by the deposition of extensive prodelta muds of SF6.

185 to 140 ka BP, early lowstand systems tract (ELST)

Higher rates of eustatic sea-level fall resulted in a forced regression of the shoreline to produce the early lowstand systems tract (ELST, Fig. 7). The first 25 ka of sea-level fall was followed by a 20 ka of prolonged stillstand of sea level. The ELST is bounded by sequence boundary 1 (SB1) below and an intra-lowstand sequence boundary (ILSB) above. A forced regressive delta, consisting of SF1, was formed during this time. Extensive intra-deltaic deformation and slope channels (SF3) incision is interpreted to have occurred during this period of fall and stillstand of eustatic sea level. We believe that extensive deformation of the deltaic deposits, as well as the increased incision of the slope channels, occurred during this prolonged stillstand of relative sea level. The shallow mass transport complex, represented by SF4, was induced at some point during this period by local uplift of the adjacent salt body, which remobilized the ELST.

140 to 130 ka, late lowstand systems tract (LLST)

The late lowstand systems tract lies between the ILSB and transgressive surface of erosion (TST). This systems tract started to form after the onset of eustatic sea level rise (Fig. 7). Slope channels (SF3) were filled and the muddier aggradational deltaic clinoform set (SF2) was formed during the LLST.

130 to 120 ka BP, transgressive systems tract (TST)

A rapid increase in sea-level rise (Fig. 7) resulted in the transgression of the shoreline and marine reworking of the underlying sediments. The transgressive systems tract is enclosed between the transgressive surface of erosion (TSE) and maximum flooding surface 2 (MFS 2), and is represented by SF5. The TST is overlain by another highstand systems tract 1 (HST1) and even younger lowstand systems tract identified as being deposited during Oxygen isotope stage 5 through 2 (Wellner et al., 2004, Suter and Berryhill, 1985).

DEFORMATION STYLES

The early lowstand forced regressive deposits of SF1 (i.e. ELST), enclosed between the sequence boundary (SB1) and transgressive surface of erosion (TST), show two types of deformation: syn-depositional growth faults and slumps, and a larger scale post-depositional slide.

Syndepositional growth faults and slumps

Growth faults are recognized on seismic lines by multiple concave downdip reflections in plan view (Fig. 8a), relatively conformable concave up surface in strike view (Fig. 8b), and concave up listric surface offsetting seismic reflections in dip view (Fig. 8c). The resulting fault plane is a scoop-shaped feature in perspective view. Growth faults observed in this study are fully contained within one depositional sequence. Spacing of the faults varies from 100 m to 500 m, and decreases in a landward direction (Fig. 8c). Fault planes range in height from below the seismic resolution (12 m), up to 100 m. Fault planes dip primarily in the direction of delta progradation (south with minor deflection towards the center of the basin). Dip angles reach 50° in the upper parts of the fault planes. The upper limits of the fault planes terminate vertically against the overlying strong reflection and occasionally within the delta complex (Figs. 8b, c). Horizontally, growth faults affect strata for distances of up to 500 m. The throw across the fault planes is on the order of 10 m. The interpretation of depositional surfaces across the faults reveals an increase in thickness and offset of the layers in the hanging walls (compare Fig. 8c with 9a). This is characteristic of syn-depositional growth faults. The growth strata of the hanging wall fan against the fault plane and are bent into a rollover anticline

26

(Fig. 9a). These faults are formed due to differential loading of denser sands over less-dense higher porosity muds during deltaic progradation, (Edwards, 1976; Bhattacharya and Davies, 2004; Wignall and Best, 2004). Growth faults activated and deformed the forced regressive delta deposits of SF1 for about 10 km landward from the maximum lowstand shoreline position. Fault planes are interpreted to terminate in the condensed section of the TST at the top, and sole into the mobile decollement layer, represented by marine muddy HST1, at the bottom. The mobility of the substrate accommodates the extension created by normal growth faults (Fig. 9a). Hanging wall strata consist of distributary mouth bar sandstones of SF1 and isolated high amplitude couplets are interpreted as channels (SF3). Extensive channeling is observed throughout the crosssection with concentrations at the bottom of hanging wall deposits, (Fig. 8c). Growth faults are capped by low amplitude ponded seismic facies interpreted as fine-grained healing facies deposited during the late lowstand of sea level accompanying the last stage of delta development (Nemec et al., 1988).
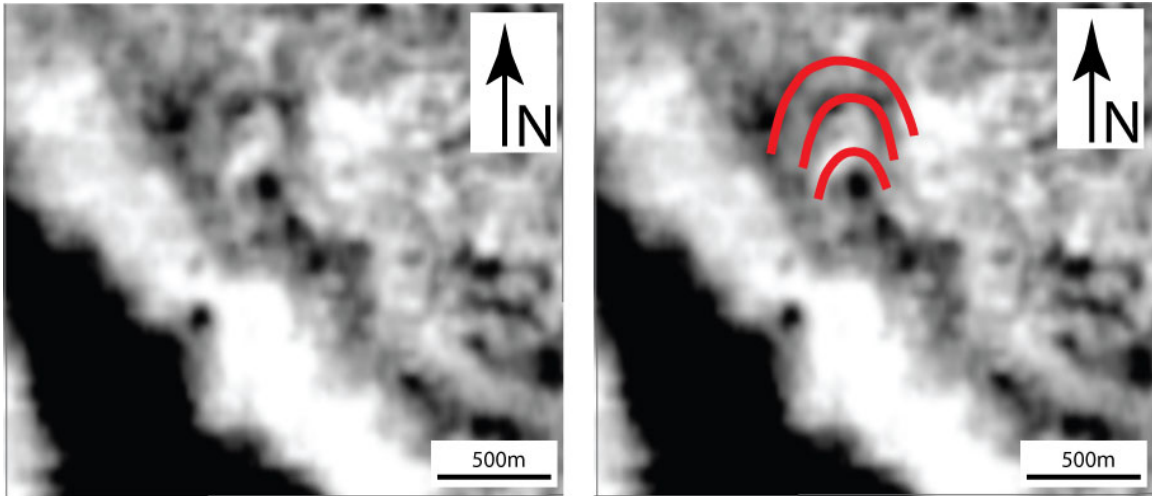
Figure 8 A. Uninterpreted and interpreted seismic amplitude timeslice at 513 ms, showing the plan view of growth faults.
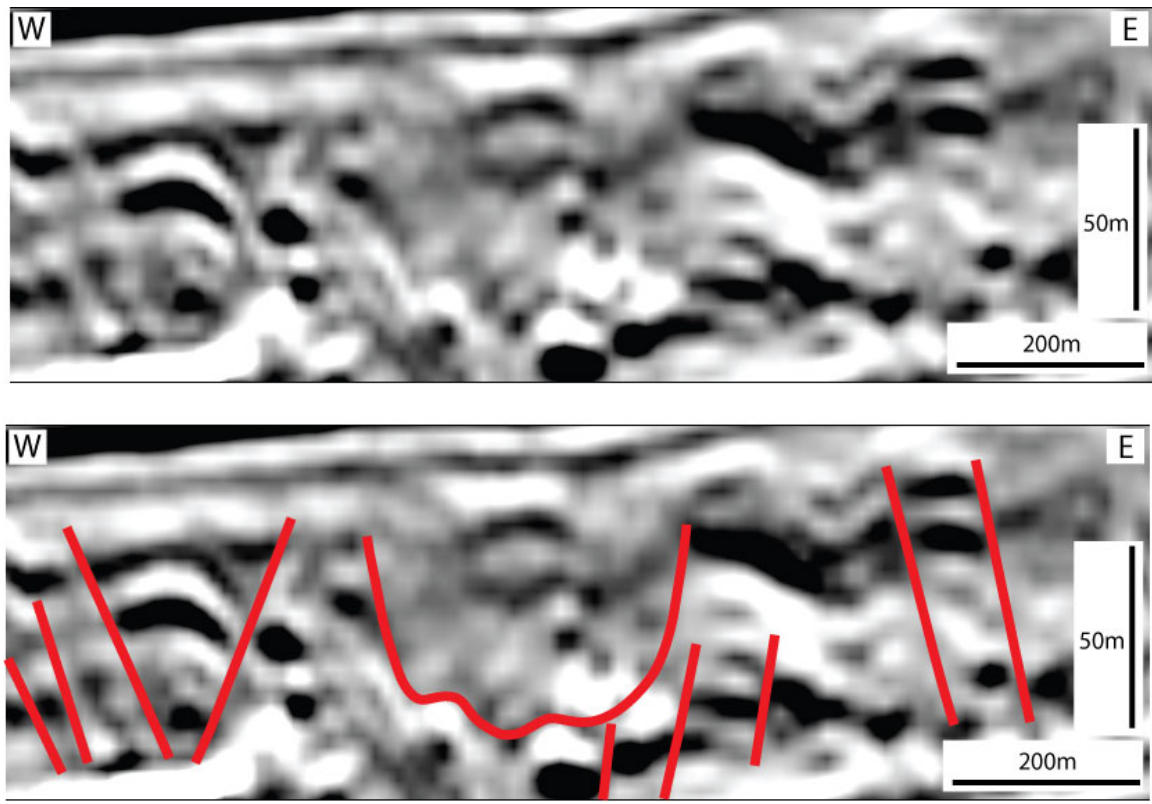
Figure 8 B. Uninterpreted and interpreted strike-oriented crosssection, showing concave-upward fault plane intersection and adjacent faults.
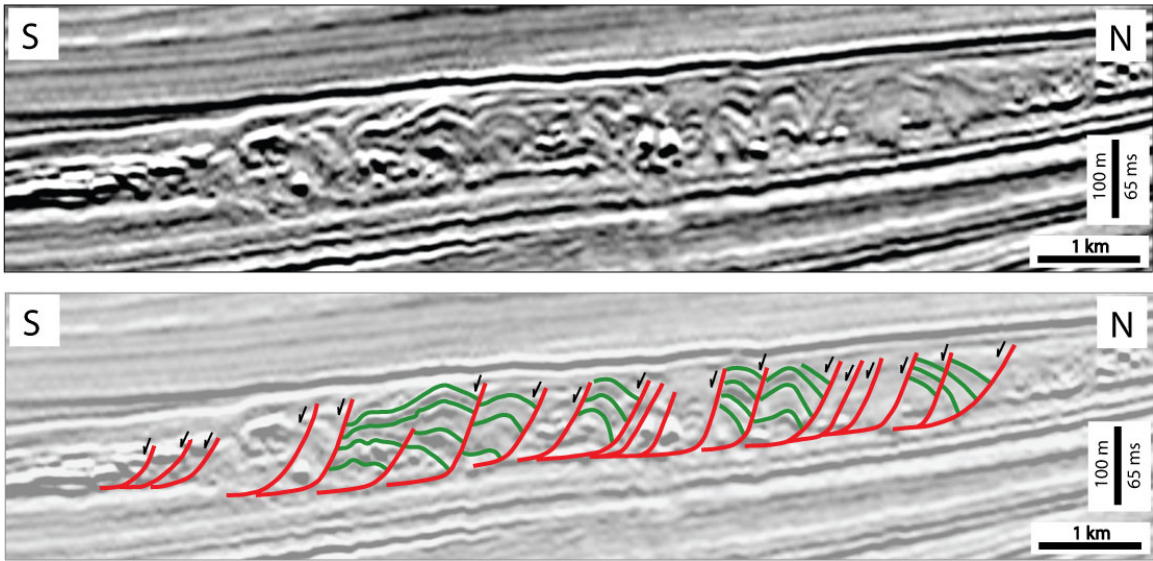
Figure 8 C. Uninterpreted and interpreted dip-oriented crosssection showing growth-fault planes in red, directions of offset and depositional layers in green.
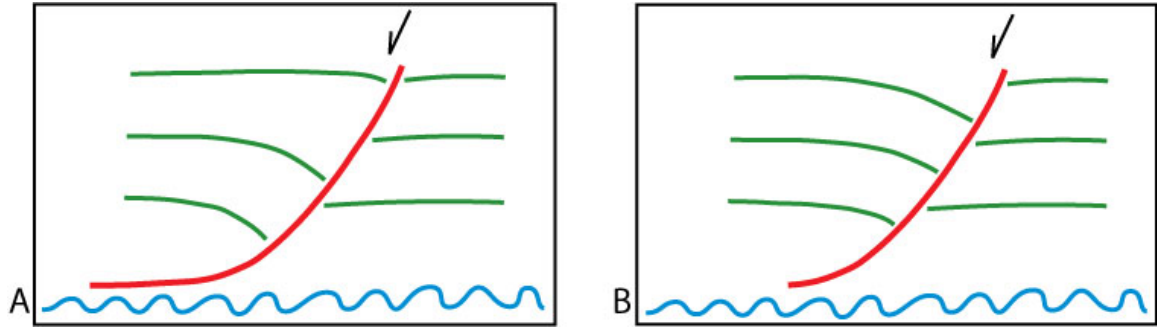
Figure 9. Schematic diagrams showing the difference in growth (A) versus non-growth (B) normal faulting. Note the progressive upward increase in the thickness of layers in the hanging walls of the growth faults (A).

Post-depositional mass transport complex (MTC)

The mass transport complex (MTC) is identified and mapped on the basis of basal and lateral erosive contacts and blocky, wavy, and chaotic low amplitude reflections of SF4 (Fig. 10a).

The direction of the deposition of the shelf-margin delta and mass transport complex is different. The former progrades to the south, whereas the latter moves to the south-east. This is supported by the observation of the north-east south-west oriented pressure ridges in the MTC (Fig. 10a). Deformation style changes along the MTC from head to toe. Fig. 10b shows a dip crosssection of the head part of the MTC. Normal faults, detaching along the basal surface, offset sediment blocks with sparsely preserved stratification. Strata on the hanging walls of the faults do not show fanning against the fault plane (compare Figs.10b and 9b). Extensional forces cause deformation as sediments are gravitationally driven down the local slope (up to 70°) created by the uplift of the salt dome to the south and west. Fig. 10c shows a dip crosssection of the central to toe part of the MTC. The stress regime is interpreted to change from extension to compression, resulting in numerous reverse faults separating folded stratified blocks and soling into the basal erosional surface. Toe thrusts are observed at the terminus of the MTC. As seen from the crosssection (Fig. 10c), regional dip of the strata is towards the center of the salt dome minibasin. The toe of the MTC had to climb the uplifted area, which impeded further movement and caused the contraction and termination of the flow. Small-scale normal faults can be seen updip from the MTC terminus, suggesting extension on the uplifted flank of the eastern salt dome. Similar cohesive slides were documented by Coleman and Prior (1983) and Morton (1993). Pressure ridges are

31

indicative of the direction and rate of movement of the slide. The distance between the adjacent pressure ridges and their degree of downdip curvature suggests that the distance of MTC progradation ranged from 1km in the head region to less than 100 m at the toe.

Although erosional edges of the MTC can be discerned from the strike-oriented crosssection (Fig. 10d), it remobilizes more than replaces the sediments of the shelf-margin delta; therefore the lithology of the sediments is mainly preserved. However, deformation causes severe disruption of the continuity and connectivity of the depositional units. Isolated slump blocks, exhibiting high amplitudes and interpreted as sands, can reach heights of up to 80 m and lengths of 700 m.
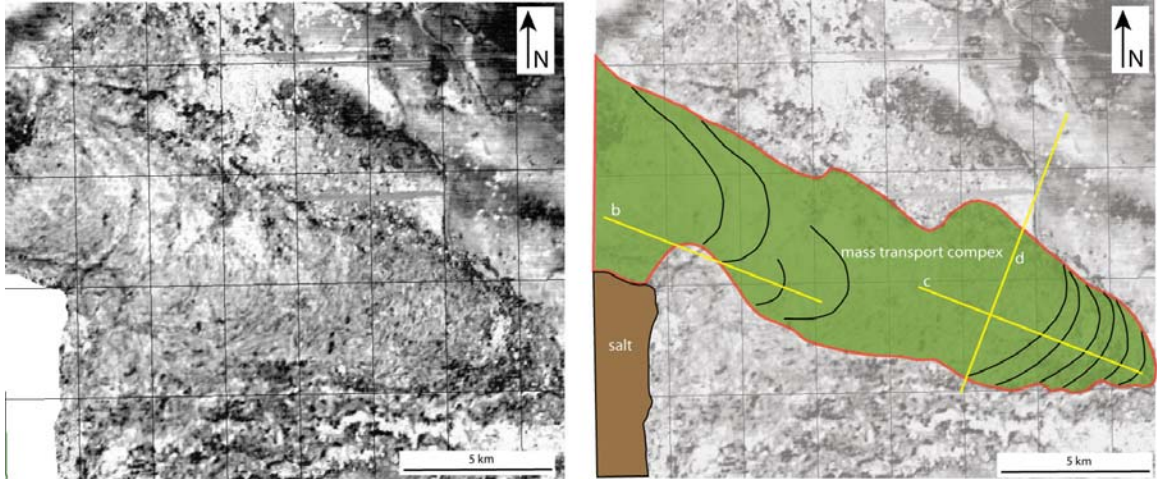
Figure 10 A. Uninterpreted and interpreted seismic amplitude horizon slice from 40ms below the maximum flooding surface. Aerial extent and the direction of flow of mass transport complex as well as locations of related cross sections are shown on the figure.
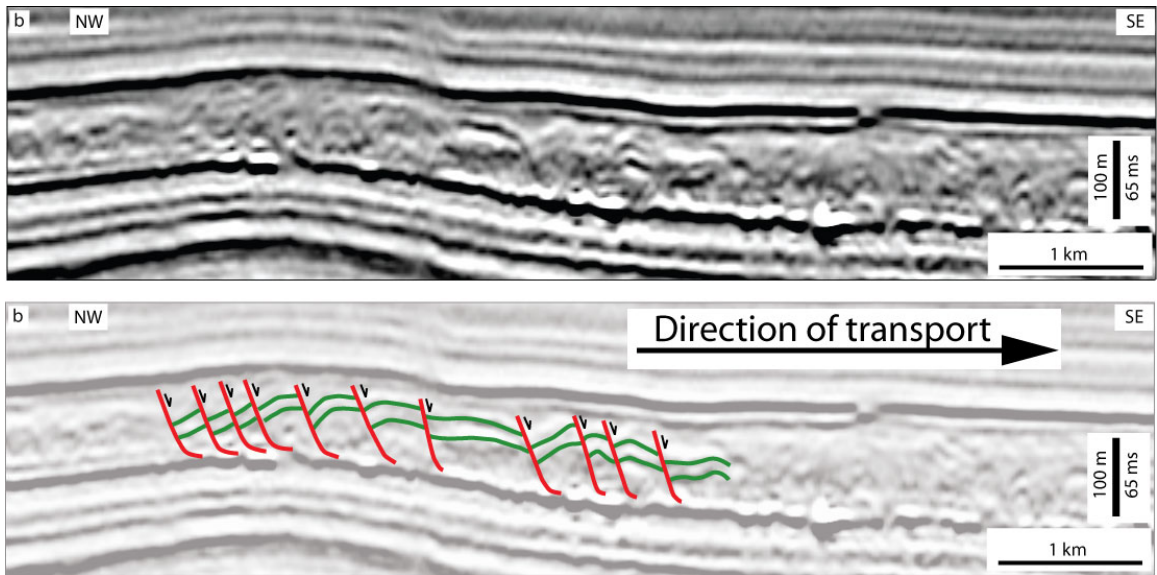
Figure 10 B. Uninterpreted and interpreted crosssection showing normal faulting at the head of the mass transport complex, extensional stress regime is interpreted at this location.
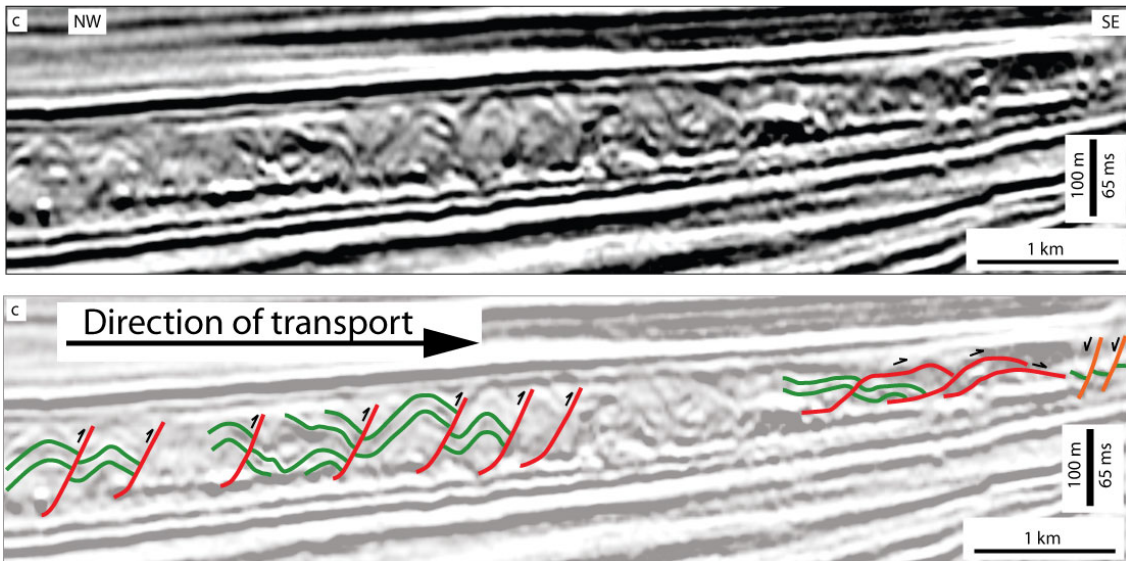
Figure 10 C. Uninterpreted and interpreted crosssection showing reverse faulting at the central part and toe thrusting at the toe of the mass transport complex, compressional stress regime is interpreted at this location. Note normal faulting updip from the terminus of the MTC resulted from the uplift of the eastern salt dome.
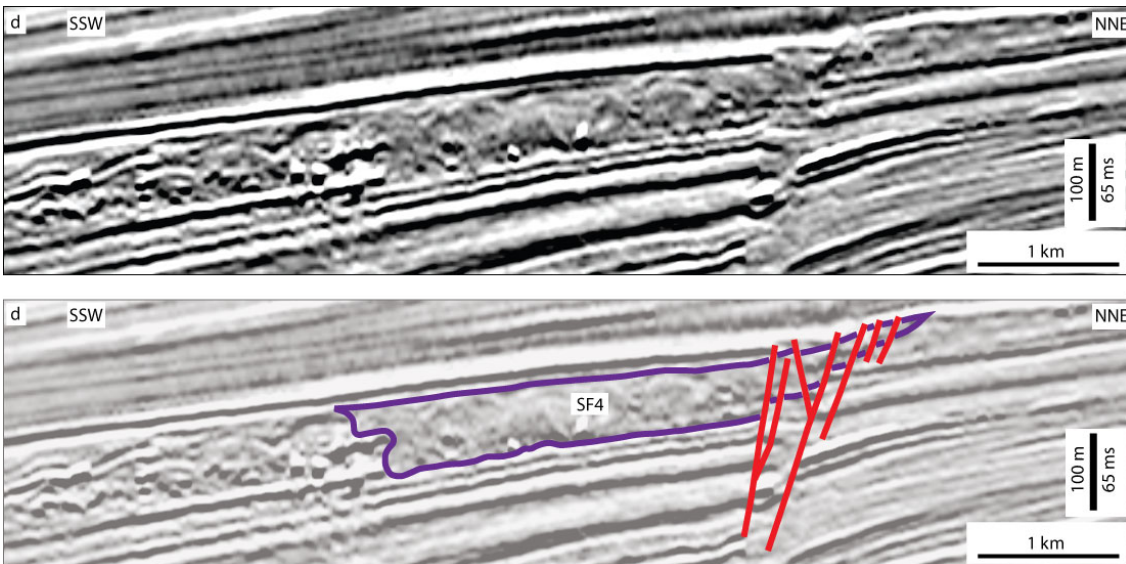
Figure 10 D. Uninterpreted and interpreted strike-oriented crosssection showing faulting at the northern boundary of the MTC and the erosional base and lateral boundary of the complex.

SHELF TO SLOPE SEDIMENT BYPASS

A series of tributive slope channels of SF3 were mapped downdip from the delta front within the early lowstand systems tracts (ELST). Slope channels were mapped at two successive times: the beginning of the forced regression at 185 ka BP (TIME 1, Figs. 11 and 12) and the ending of the forced regression at 140 ka BP, (TIME 2, Figs. 13 and 14). Western and eastern slope channel complexes are recognized. Widths of the channels vary from 100 m to 400 m, their maximum sinuosity is 1.03. The depth of incision increases basinward and ranges from 15 m to 100 m. Levees are not observed at the channel banks, suggesting full confinement of flows. Channels appear to be initiated at the delta lobes or at the basinward limits of the low amplitude areas located downdip from the delta lobes. These areas are characterized by concave basinward scars, followed by curved low amplitude, incoherent reflections repeating the shape of the scar. These features are interpreted as delta-front slumps.

At TIME 1, when the shelf-margin delta reached the position of the older shelf edge (Figs. 11 and 12), delta-front turbidites are hypothesized to have caused the incision and formation of the slope channels. These slope channels exhibit a tributive pattern. Dominant slope channels formed within both western and eastern channel networks, and are marked by the increased width and depth of incision.

TIME 2 marks the end of the shelf-margin delta progradation into the basin (Figs. 13 and 14). The shelf edge has moved some 5 km basinward. Slope channels were progressively overlain by the prograding delta clinoforms with probable delta-front turbidites occupying previously incised channels and increasing the depth of incision. Slope channels mapped at TIME 2 are fewer in number, wider, and more deeply incised.

The fluvial-dominated nature of the shelf-margin delta prograding under conditions of high sediment supply and rapid eustatic sea-level fall supports the idea of the initiation of the delta-front turbidites by two processes: 1) direct link with subaerial distributary channels, and 2) delta-front slumps. The former process is hypothesized to produces more continuous and lasting flows than the latter. In both cases, fluvial and deltaic sediments are likely delivered to the slope and possibly basin floor via slope channels. Our data suggests that both processes were operative, as indicated by the presence of both slump- and distributary channel-fed channels.
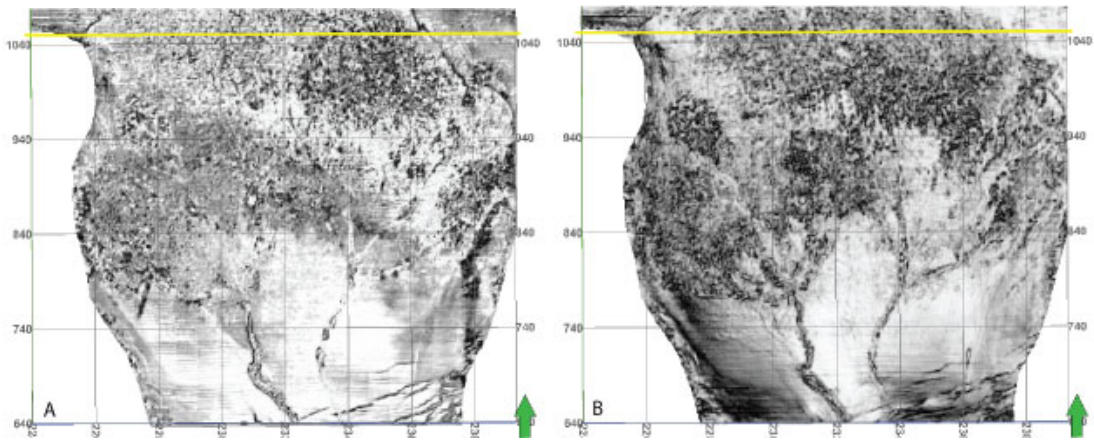
Figure 11 (A) Amplitude horizon slice 8 ms above the sequence boundary and (B) Amplitude horizon slice 16 ms above the sequence boundary. Slumping at the delta front and slope channel network is interpreted from these horizon slices.
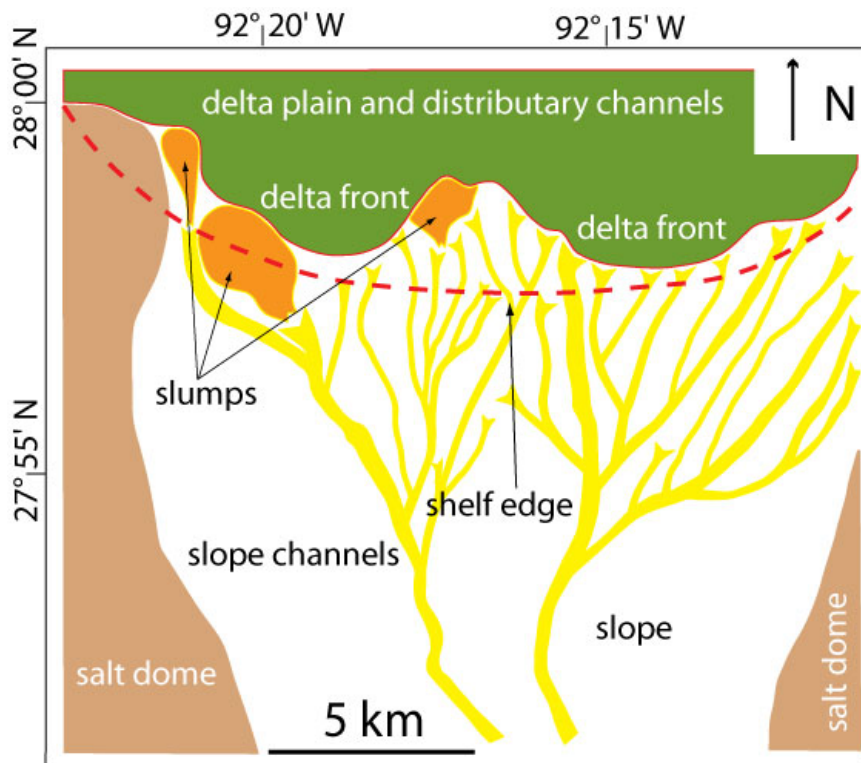
Figure 12. Paleogeologic map of the study area at TIME 1, some time before the end of the forced regression.
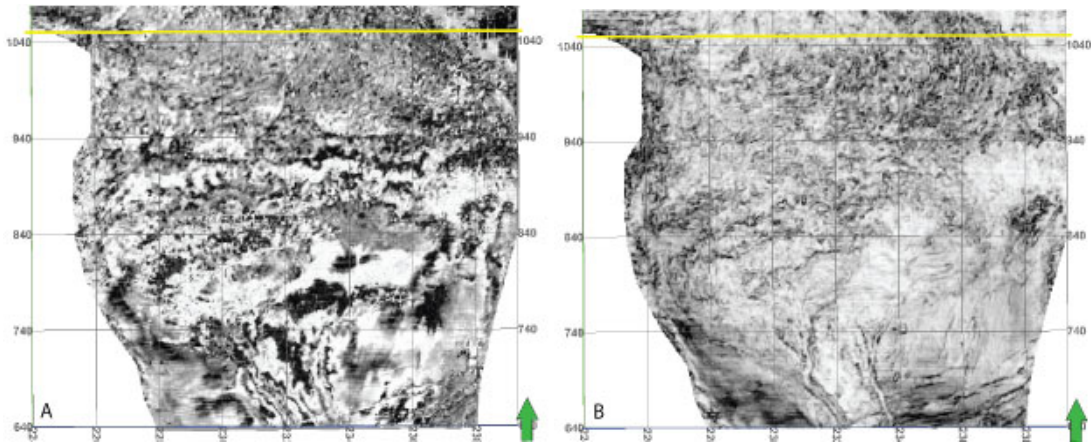
Figure 13 (A) Amplitude horizon slice 48 ms below the transgressive surface of erosion and (B) Variance horizon slice 32 ms below the transgressive surface of erosion. Delta lobes, slope channels, and slumps are interpreted from these horizon slices.
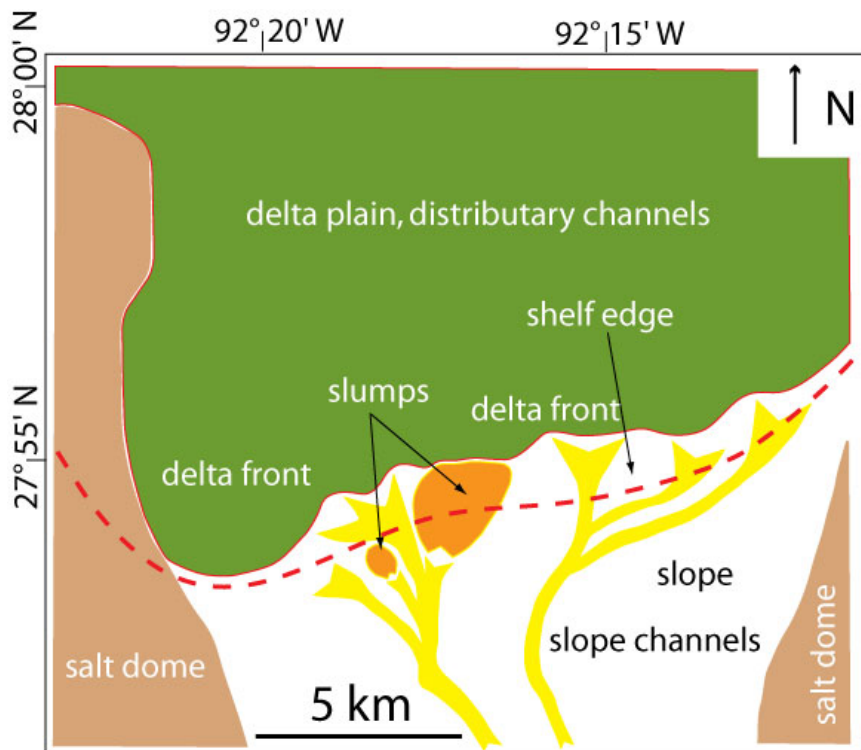
Figure 14. Paleogeologic map of the study area at TIME 2, at the end of the forced regression.

DISCUSSION

Among the 4 deltaic complexes within the upper kilometer of the salt dome minibasin fill (Fig. 4), complex 2 exhibits the highest degree of intra- and extra-deltaic deformation as well as the incision of the slope channels. We hypothesize that the prolonged lowstand of eustatic sea level, lasting 45 ka, is one of the major factors that allowed the complex to be deformed and fluvio-deltaic sediment to be transported beyond the shelf edge via slope channels. The lithology of bypassed sediments depends on the staging area, as well as the process of the initiation of delta-front turbidites (Posamentier and Walker, 2006). Delta-front turbidites may be formed by distributary channels reaching the shelf edge, by slumping at the delta front due to sediment instability, or by storms or earthquakes. Low compaction of rapidly deposited sediments, excessive pore fluid pressures, high water, and free gas contents are all factors that may reduce the shear strength of the sediments and contribute to instability at the delta front (Coleman and Prior, 1983). Delta-front slumping is observed in the western slope channel network exclusively. This could possibly be a consequence of the higher magnitude of the western salt dome uplift and resulting increase in the local sea-floor gradient. We predict higher sand content of the sediment transported to the slope in the western systems, where occasional slumps are present. The reason lies in the notion that slumps activate coarser grained, delta-front sediments that were staged at the shelf margin, whereas delta-front turbidites fed by distributary channels probably carry a higher proportion of mud, presumably reflecting the sediment load of the rivers, which would be transported directly downdip (Bhattacharya, 2006).

39

Growths faults observed in this study compare favorably with the smaller scale outcrop examples of intra-parasequence growth faulting, described by Bhattacharya and Davies (2004), Wignall and Best (2004), and Nemec et al. (1988), as opposed to the much larger scale regional growth faults of the Gulf of Mexico and the Niger delta documented by Diegel et al. (1995) and Evamy et al. (1978) respectively. Thus growth faults described in this work represent a direct analog to the "subseismic", or intra-formational growth faults that are potentially significant in reservoir heterogeneity of river-dominated deltas (e.g. Tye et al., 1999). The similarity of our faults to the ones described by Bhattacharya and Davies (2004) and Wignall and Best (2004) suggests a similar depositional environment and formation mechanism. All deltas described by these authors are river dominated with high sediment supply. The presence of multiple lobes and growth faults in our delta supports the idea of high sedimentation rates and fluvial dominance during the delta formation.

Our data also suggests that external morphology is not a reliable indicator of the internal facies architecture. Horizon slices and paloegeologic maps from Figures 11, 12, 13, and 14 suggest that the delta front approximated the paleoshoreline and thus resembles wave-dominated delta morphology, whereas the internal architecture indicates fluvial dominance at the time of deposition.

A model for the stratigraphic architecture of shelf-margin deltas proposed by Porebski and Steel (2003) is compared to the one constructed based on the present study (Fig. 15). In our model, late lowstand systems tract deposits are less thick and have thick onlapping transgressive deposits. The base of the sequence has an erosive nature caused by both slope gullying and mass transport movements (Fig. 15).

40
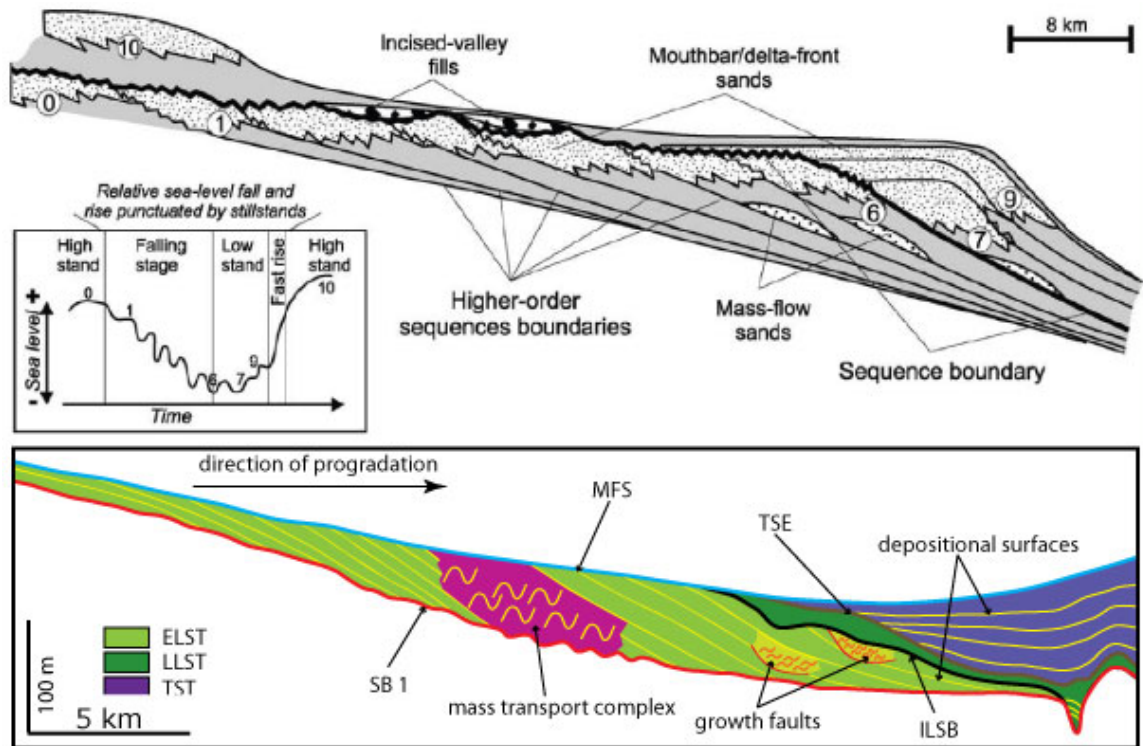
Figure 15. Schematic diagram of the sequence stratigraphy of the delta from Porebski and Steel (2003) is compared with our diagram. Note thinner late lowstand systems tract deposits, and much thicker transgressive deposits.

CONCLUSIONS

- 3D seismic data allow evaluation of the seismic stratigraphy, seismic geomorphology, and internal facies heterogenity of a Pleistocene shelf-margin delta within a salt dome mini-basin, in offshore Louisiana. The delta consists of a series of offlapping sandy clinoforms, interpreted as being associated with a prolonged forced-regression and ensuing lowstand of sea level, associated with Oxygen isotope stage 6, which lasted about 20Ky.

- The lowstand delta consists of early lowstand, down-stepping forced regressive sandy clinoforms, followed by a set of aggrading muddier clinoforms, interpreted as a late lowstand. The early and late lowstand systems are separated by an intra-lowstand sequence boundary. The lowstand delta is onlapped by a thick transgressive mud wedge that would represent a potential sealing facies, and is underlain and capped by regionally persistent highstand mudstones.

- The lowstand phase consists of multiple lobate sediment bodies, suggesting the delta was built primarily from coalescing, fluvial-dominated mouth bars. Despite the shelf-edge position, there is no evidence of wave-reworked sand bodies, such as linear strandplains, and the delta does not appear to be wave-influenced.

- The adjacent shelf edge and slope contain well-imaged tributive channels, downdip of the delta front. These are interpreted as submarine slope channels, some of which are connected with updip distributary channels, and are interpreted to have formed near the end of the prolonged lowstand. These channels have a high potential for transporting coarse-grained sediment down the slope and onto the basin floor. There

is also evidence that some of the slope channels are fed by slumps towards the western margin of the minibasin, which is more active in terms of the salt tectonics.

- Two types of soft-sediment deformation are observed. In the central parts of the delta. Syn-sedimentary intra-deltaic deformation is indicated by a series of small growth faults, fully contained within the delta, and with throws of about 10 m. The growth faults are also likely related to the river-dominated nature of the delta, characterized by rapidly deposited, mobile prodelta muds over which delta-front sands were deposited, triggering the faults.

- The central part of the delta also shows post-depositional deformation caused by a shallow-water mass transport complex (MTC) that remobilizes the deltaic deposits. The MTC shows well-defined pressure ridges and forms two lobate complexes that truncate the adjacent clinoform delta deposits. The MTCs flow almost perpendicular to the direction of the regional delta progradation that it replaces. The shallow mass transport complex is interpreted to have formed in water depths of around 100 m and was likely induced by the uplift of the adjacent western salt dome, although we believe that it has traveled less that 1 km along the central part of the mini-basin.

- We hypothesize that the high degree of syn- and post-depositional deformation, as well as the well-developed shelf-edge channel-networks are related to the prolonged nature of the lowstand, as well as the fact that the delta is highly river-dominated. In contrast, shelf-edge deltas formed during shorter-term eustatic drops, or which are more wave-influenced, seem to lack the deformation features. Despite being deposited in an area of active salt tectonics, growth strata are largely confined within the delta complex, in contrast to regional growth faults that offset numerous stacked

43

complexes in the western Gulf of Mexico and in other shale-cored systems like the Niger deltas.

- The confinement of this delta, between thick transgressive and highstand prodelta mudstones, suggests that shelf-margin deltas could form an ideal reservoir seal pair, although the intra-deltaic facies complexity (clinoforms and fluvial-dominated mouth bars) and soft-sediment deformation would result in an extremely complex reservoir.

REFERENCES CITED

Abdulah, K.C., Anderson, J.B., Snow, J.N., and Holdford-Jack, L., 2004, The Late Quaternary Brazos and Colorado deltas, offshore Texas, U.S.A.-their evolution and the factors that controlled their deposition, *in* Anderson, J.B., and Fillon, R.H., eds., Late Quaternary Stratigraphic Evolution of the Northern Gulf of Mexico Margin: SEPM, Special Publication 79, p.237-269.

Abreu, V., Sullivan, M., Pirmez, C., and Mohrig, D., 2003, Lateral accretion packages (LAPs): an important reservoir element in deep water sinuous channels: Marine and Petroleum Geology, v. 20, p. 631–648.

Alexander, L.L., and Flemings, P.B., 1995, Geologic evolution of a Pliocene-Pleistocene salt-withdrawal minibasin: Eugene Island Block 330, Offshore Louisiana: AAPG Bulletin, v. 79, no. 12, p. 1737-1756.

Anderson, J.B., Rodriguez, A., Abdulah, K.C., Fillon, R.H., Banfield, L.A., McKeown, H.A., and Wellner, J.S., 2004, Late Quaternary stratigraphic evolution of the Northern Gulf of Mexico margin: A synthesis, *in* Anderson, J.B., and Fillon, R.H., eds., Late Quaternary Stratigraphic Evolution of the Northern Gulf of Mexico Margin: SEPM, Special Publication 79, p. 1-23.

Beaubouef, R. T., and S. J. Friedmann, 2000, High resolution seismic/sequence stratigraphic framework for the evolution of Pleistocene intra slope basins, western Gulf of Mexico: Depositional models and reservoir analogs, *in* P. Weimer, R. M. Slatt, J. Coleman, N. C. Rosen, H. Nelson, A. H. Bouma, M. J. Styzen, and D. T. Lawrence, eds., Deep-water reservoirs of the world: Gulf Coast Section SEPM 20th Annual Research Conference, p. 40–60.

Berg, O.R., 1982, Seismic detection and evaluation of delta and turbidite sequences: their application to exploration for the subtle trap: AAPG Bulletin, v. 66, no. 9, p. 1271-1288.

Berryhill et al., 1986, Late Quaternary facies and structure, Northern Gulf of Mexico, Interpretations from seismic data: AAPG Studies in Geology # 23.

Bhattacharya, J.P., 2006, Deltas, *in* Posamentier, H., and Walker, R.G., eds., Facies Models Revisited: SEPM, Special Publication 84, p. 237–292.

Bhattacharya, J.P., and Giosan, L., 2003, Wave-influenced deltas: geomorphological implications for facies reconstruction: Sedimentology, v. 50, p. 187–210.

Bhattacharya, J.P., and Walker, R.G., 1992, Deltas, *in* Walker, R.G., and James, N.P., eds., Facies Models: Response to Sea Level Change: St. John's, Newfoundland, Geological Association of Canada, p. 157–177.

45

Bhattacharya, J.P. and Davies, R.K., 2004, Sedimentology and structure of growth faults at the base of the Ferron Sandstone Member along Muddy Creek, Utah, *in* Chidsey, T.C., Adams, R.D., and Morris, T.H., eds., The Fluvial-Deltaic Ferron Sandstone: Regional-to-wellbore-scale outcrop analog studies and applications to reservoir modeling: AAPG, Studies in Geology 50, p. 279-304.

Brami, T. R., C. Pirmez, C. Archie, and K. Holman, 2000, Late Pleistocene deep-water stratigraphy and depositional processes, offshore Trinidad and Tobago, *in* P. Weimer, R. M. Slatt, J. Coleman, N.C. Rosen, H. Nelson, A.H. Bouma, M.J. Styzen, and D. T. Lawrence, eds., Deep-water reservoirs of the world: Gulf Coast Section SEPM 20th Annual Research Conference, p. 104–115.

Bridge, J.S., 2003, Rivers and Floodplains; Forms, Processes, and Sedimentary Record: Oxford, U.K., Blackwell Science, 504 p.

Brown, A.R., 2004, Interpretation of Three Dimensional Seismic Data: The American Association of Petroleum Geologists and the Society of Exploration Geophysicists, Tulsa, OK, 535.

Coleman, J.M., and Wright, L.D., 1975, Modern river deltas: variability of processes and sand bodies, in Broussard, M.L., ed., Deltas; Models for Exploration: Houston Geological Society: Houston, p. 99–149.

Coleman, J. M., D. B. Prior, and J. F. Lindsay, 1983, Deltaic influences on shelf edge instability processes, *in* D. J. Stanley and G. T. Moore, eds., The shelf break; critical interface on continental margins: SEPM Special Publication 33, p. 121–138.

Diegel, F. A., J. F. Karlo, D. C. Schuster, R. C. Shoup, and P. R. Tauvers, 1995, Cenozoic structural evolution and tectono-stratigraphic framework of the northern Gulf Coast continental margin, *in* M. P. A. Jackson, D. G. Roberts, and S. Snelson, eds., Salt tectonics: a global perspective: AAPG Memoir 65, p. 109–151.

Davies, R.J., Posamentier, H.W., Wood, L.J., and Cartwright, J.A. (eds) 2007. Seismic Geomorphology: Applications to Hydrocarbon Exploration and Production. Geological Society, London, Special Publications, **277**.

Edwards, M. B., 1976, Growth faults in upper Triassic deltaic sediments, Svalbard: AAPG Bulletin, v. 60, p. 341–355.

Evamy, D. D., J. Haremboure, P. Kamerling, W. A. Knapp, F. A. Molloy, and P. H. Rowlands, 1978, Hydrocarbon habitat of Tertiary Niger delta: AAPG Bulletin, v. 62, p. 1–39.

Fielding, C.R., Trueman, J., and Alexander, J., 2005, Sedimentology of the modern and Holocene Burdekin River Delta of north Queensland, Australia—controlled by river output, not by waves and tides, *in* Giosan, L., and Bhattacharya, J.P., eds., River Deltas: Concepts, Models, and Examples: SEPM, Special Publication 83, p. 467–496.

Galloway, W.E., 1975, Process framework for describing the morphologic and stratigraphic evolution of deltaic depositional systems, *in* Broussard, M.L., ed., Deltas; Models for Exploration: Houston Geological Society: Houston, p. 87–98.

Galloway, W.E., and Hobday, D.K., 1996, Terrigenous Clastic Depositional Systems: Heidelberg, Springer-Verlag, 489 p.

Galloway, W.E., Ganey-Curry, P.E., Li, X., and Buffler, R.T., 2000, Cenozoic depositional history of the Gulf of Mexico basin: AAPG Bulletin, v. 84, no. 11, p. 1743-1774.

Gani, M.R., and Bhattacharya, J.P., 2005, Lithostratigraphy versus chronostratigraphy in facies correlations of Quaternary deltas: application of bedding correlation, *in* Giosan, L., and Bhattacharya, J.P., eds., River Deltas: Concepts, Models, and Examples: SEPM, Special Publication 83, p. 31–48.

Hart, B.S., and Long, B.F., 1996, Forced regressions and lowstand deltas: Holocene Canadian example: Journal of Sedimentary Research, v. 66, p. 820–829.

Helland-Hansen, W., and Gjelberg, J.G., 1994, Conceptual basis and variability in sequence stratigraphy: a different perspective: Sedimentary Geology, v. 92, p. 31-52.

Imbrie, J., Hays, J.D., Martinson, D.G., 1984, The orbital theory of Pleistocene climate: Support from a revised chronology of the marine oxygen isotope record, in Berger, A.L., ed., Milankovitch and Climate: Dordrecht, The Netherlands, Reidel Publishing Company, p. 269-305.

Lambiase, J.J., Damit, A.R., Simmons, M.D., Abdoerrias, R., and Hussin, A., 2003, A depositional model and the stratigraphic development of modern and ancient tide-dominated deltas in NW Borneo, *in* Sidi, F.H., Nummedal, D., Imbert, P., Darman, H., and Posamentier, H., eds., Tropical Deltas of Southeast Asia: Sedimentology, Stratigraphy, and Petroleum Geology: SEPM, Special Publication 76, p. 109–123.

Mellere, D., Plink-Bjorklund, P., and Steel, R., 2002, Anatomy of shelf deltas at the edge of a prograding Eocene shelf margin, Spitsbergen: Sedimentology, v. 49, p. 1181–1206.

Morton, R. A., 1993, Attributes and origins of ancient submarine slides and filled embayments: examples from the Gulf Coast basin: AAPG Bulletin, v. 77, no. 6, p. 1064–1081.

Moscardelli, L., Wood, L., and Mann, P., 2006, Mass-transport complexes and associated processes in the offshore area of Trinidad and Venezuela: AAPG Bulletin, v. 90, no. 7, p. 1059-1088.

Mulder, T., and Syvitski, J.P.M., 1995, Turbidity currents generated at mouths of rivers during exceptional discharges to the world oceans: Journal of Geology, v. 103, p. 285–299.

Nemec, W., R. J. Steel, J. Gjelberg, J. D. Collinson, E. Prestholm, and I. E. Oxnevad, 1988, Anatomy of a collapsed and re-established delta front in Lower Cretaceous of Eastern Spitsbergen — gravitational sliding and sedimentation processes: AAPG Bulletin, v. 72, p. 454–476.

Olariu, C., and Bhattacharya, J.P., 2006, Terminal distributary channels and delta front architecture of river-dominated delta systems: Journal of Sedimentary Research, v. 76, p. 212–233.

Plink-Bjorklund, P., and Steel, R., 2005, Deltas on falling-stage and lowstand shelf margins, the Eocene Central Basin of Spitsbergen: Importance of sediment supply, *in* Giosan, L., and Bhattacharya, J.P., eds., River Deltas: Concepts, Models, and Examples: SEPM, Special Publication 83, p. 179–206.

Porebski, S.J. and Steel, R.J., 2006, Deltas and sea level change: Journal of Sedimentary Research, v. 76, p. 390-403.

Posamentier, H. W., and V. Kolla, 2003, Seismic geomorphology and stratigraphy of depositional elements in deep water settings: Journal of Sedimentary Research, v. 73, no. 3, p. 367–388.

Posamentier, H.W., and Allen, G.P., 1999, Siliciclastic Sequence Stratigraphy—Concepts and Applications: Society of Economic Paleontologists and Mineralogists, Concepts in Sedimentology and Paleontology #7, 210 p.

Posamentier, H., and Walker, R.G., eds., 2006, Facies Models Revisited: SEPM, Special Publication 84

Prather, B.E., Booth, J.R., Steffens, G.S., and Craig, P.A., 1998, Classification, lithologic calibration and stratigraphic succession of seismic facies of intraslope basins, deep-water Gulf of Mexico: AAPG Bulletin, v. 82, p. 701–728.

Roberts, H.H., Fillon, R.H., Kohl, B., Robalin, J.M., and Sydow, J.C., 2004, Depositional architecture of the Lagniappe delta: sediment characteristics, timing of depositional events, and temporal relationship with adjacent shelf-edge deltas, *in* Anderson, J.B., and Fillon, R.H., eds., Late Quaternary Stratigraphic Evolution of the Northern Gulf of Mexico Margin: SEPM, Special Publication 79, p. 143-188.

Rodriguez, A.B., Hamilton, M.D., and Anderson, J.B., 2000, Facies and evolution of the modern Brazos Delta, Texas: wave versus flood influence: Journal of Sedimentary Research, v. 70, p. 283–295.

Salvador, A., 1987, Late Triassic-Jurassic paleogeography and origin of Gulf of Mexico basin: AAPG Bulletin, v. 71, no. 4, p. 419-451.

Suter, J. R., and H. L. Berryhill, Jr., 1985, Late Quaternary shelf-margin deltas, northwest Gulf of Mexico: AAPG Bulletin, v. 69, p. 77–91.

Sydow, J., and Roberts, H.H., 1994, Stratigraphic framework of a late Pleistocene shelf-edge delta, northeast Gulf of Mexico: AAPG Bulletin, v. 78, p. 1276–1312.

Vail, P.R., Mitchum, R.M., Todd, R.G., Widmier, J.M., Thompson, S., Sangree, J.B., Bubb, J.N., and Hatlelid, W.G., 1977, Seismic stratigraphy and global changes of sea level, *in* C. E. Payton, ed., Seismic Stratigraphy - Applications to Hydrocarbon Exploration: AAPG Memoir 26, p. 49-213.

Van Heerden, I.L. and Roberts, H.H., 1988, Facies development of Atchafalaya delta, Louisiana: A modern bayhead delta: AAPG Bulletin, v. 72, no. 4, p. 439-453.

Wellner, J.S., Sarzalejo, S., Lagoe, M., and Anderson, J.B., 2004, Late Quaternary stratigraphic evolution of the West Louisiana/East Texas continental shelf, *in* Anderson, J.B., and Fillon, R.H., eds., Late Quaternary Stratigraphic Evolution of the Northern Gulf of Mexico Margin: SEPM, Special Publication 79, p. 217-235.

Wignall, P.B., and Best, J.L., 2004, Sedimentology and kinematics of a large, retrogressive growth-fault system in Upper Carboniferous deltaic sediments, western Ireland: Sedimentology, v. 52, p. 1343-1358.

Winker, C. D., and M. B. Edwards, 1983, Unstable progradational clastic shelf margins, *in* D. J. Stanley and G. T. Moore, eds., The shelf-break — critical interface on continental margins: SEPM Special Publication 33, 139–157.

Wood, L.J., 2007, Quantitative seismic geomorphology of Pliocene and Miocene fluvial systems in the Northern Gulf of Mexico, U.S.A.: Journal of Sedimentary Research, v. 77, 713-730.